Hindawi
Advances in Civil Engineering
Volume 2024, Article ID 8878093, 13 pages
https://doi.org/10.1155/2024/8878093

Research Article

Improved Deflection Prediction Model for PSC Box Girder with Stay Cable System during Tensioning Phase

Gangnian Xu,[1] **Weimin Xu**,[2] **Zhanhong Wang**,[3] **and Ruishuo Zhang**[1]

[1]*School of Transportation and Civil Engineering, Shandong Jiaotong University, Jinan 250357, China*
[2]*Jinan Urban Construction Group, Jinan 250102, China*
[3]*Railway Baoji Bridge Group Co. Ltd., Baoji 721006, China*

Correspondence should be addressed to Gangnian Xu; xugangnian2007@163.com

Received 25 April 2023; Revised 7 November 2023; Accepted 4 December 2023; Published 11 January 2024

Academic Editor: Melina Bosco

To improve the accuracy of deflection prediction for prestressed concrete (PSC) box-girder bridges with a stay cable system (SCS) during tensioning, this study employs the Latin hypercube sampling (LHS) technique to sample random variables affecting long-term deflection of the main girder. A long-term deflection randomness analysis model is established, and the shear stiffness degradation factor is included to quantify the contribution of diagonal web cracking to the main girder deflection. Uncertainty and sensitivity analysis are conducted for the Dongming Huanghe River Highway Bridge. An objective function is applied to select the optimal combination of random variables, and a modified model is established and verified for accuracy. Results show that diagonal web-cracking accounts for 8.8% of total deflection and cannot be ignored, and the prestressed tension control stress, creep uncertainty coefficient, and concrete density significantly impact long-term deflection. The modified model predicts deflection with greater accuracy than the mean value model.

1. Introduction

The calculation of deflection in bridge structures currently involves various methods, including theoretical analysis, model testing, and numerical simulations. However, theoretical analysis and model testing have limitations, especially when it comes to analyzing existing bridges. As a result, many researchers turn to the finite element (FE) method as a commonly used approach. Nonetheless, numerous studies rely on the fixed-value design method for analyzing the long-term deflection of prestressed concrete (PSC) continuous box-girder bridges, neglecting uncertainties associated with concrete properties, steel tendon materials, and box-girder geometry [1, 2].

To address this uncertainty issue, previous research has applied the FE method and selected random variables that influence concrete shrinkage, creep, or prestress loss when analyzing the main girder deflection in PSC box-girder bridges [3, 4]. However, the analysis of large-span PSC continuous box-girder bridges presents challenges, such as complex FE models, numerous elements, high-computational complexity, and reduced efficiency. Many researchers opt for structural symmetry to simplify their studies, but this approach does not account for variations in the degree of damage in each span, like diagonal web cracking and shear stiffness degradation. Hence, FE modeling should not be simplistically treated as a symmetric structure.

Furthermore, diagonal web cracking is a common stress-related issue in long-span PSC continuous girder bridges, contributing to downward deflection that cannot be overlooked [5]. Past studies have shown that we must consider the downward deflection stemming from shear stiffness degradation. Determining the factors influencing downward deflection involves taking into account the actual construction processes and measured data, and applying a fixed-value analysis method. These factors include the segmental construction method, cross-sectional dimensions of the box girder, secondary dead load, residual prestress value of the external tendons, and stiffness degradation of the main girder after cracking.

Although the use of a stay cable system (SCS) reinforcement method effectively addresses midspan deflection and

beam cracking, the accuracy of deflection prediction in PSC box-girder bridges enhanced by SCS during the tensioning phase is not always satisfactory. In response, this study proposes an uncertainty analysis method based on a truss model for the time-dependent deflection of long-span PSC continuous box-girder bridges with diagonal web-cracking damage. This method was employed to conduct uncertainty and sensitivity analyses of the long-term deflection of the main girder of the Dongming Huanghe River Highway Bridge. An objective function was used to select the optimal combination of random variables, leading to the establishment and verification of a modified model suitable for predicting the long-term deflection of PSC box girders enhanced by SCS during the tensioning phase, with enhanced accuracy.

2. Uncertainty Model for Aging Deflection of PSC Continuous Girder Bridges

2.1. Shrinkage and Creep Forecast of Concrete. The CEB-FIP [6] model is a widely employed method for analyzing the long-term deflection of concrete structures, considering the effects of shrinkage and creep. The uncertainty in creep models primarily arises from variations in the creep degree function [7].

$$\varepsilon(t, t_0) = \alpha_1 \sigma J(t, t_0) + \alpha_2 \varepsilon_{sh}(t, t_0), \tag{1}$$

$$J(t, t_0) = \frac{1}{E_c(t_0)} + \frac{\phi(t, t_0)}{E_{c28}}, \tag{2}$$

where α_1 denotes the random influence factor related to the uncertainty in creep, while α_2 represents a random influence factor associated with contraction uncertainty; σ stands for constant uniaxial compressive stress of concrete; $J(t, t_0)$ represents the creep function; $\varepsilon_{sh}(t, t_0)$ is the shrinkage strain; $E_c(t_0)$ is the modulus of elasticity at the concrete age of t_0, E_{c28} corresponds to the elastic modulus of concrete at 28 days, and $\phi(t, t_0)$ is the creep coefficient. The creep coefficient is determined using a hyperbolic power function as follows:

$$\phi(t, t_0) = \left[1 + \frac{1 - RH/RH_0}{0.46(h/100)^{1/3}}\right]\left(\frac{5.3}{\sqrt{0.1 f_{cm28}}}\right)\left(\frac{1}{0.1 + t_0^{1/5}}\right)\left[\frac{t - t_0}{\beta_H + (t - t_0)}\right]^{0.3}, \tag{3}$$

where RH is the relative environmental humidity, RH_0 is equal to 100%; h denotes the nominal size of the concrete member, defined as $2A_c/u$, mm; A_c represents the cross-sectional area, mm^2; u is the perimeter in contact with the atmosphere, mm; f_{cm28} stands for the mean compressive strength at the age of 28 days, MPa; β_H is defined as $150[1 + (1.2RH)^{18}\frac{h}{100} + 250 \leq 1500$.

Over time, the predicted value of concrete strength becomes:

$$f_{cm}(t) = \beta_{cc}(t) f_{cm28}, \tag{4}$$

$$\beta_{cc}(t) = \exp\left[s\left(1 - \sqrt{28/t_{eq}}\right)\right], \tag{5}$$

where $\beta_{cc}(t)$ = a time-dependent coefficient; based on the differences between rapid hardening and early strength, ordinary rapid hardening, and slow hardening of cement, s is taken as 0.2, 0.25, and 0.38, respectively. The equivalent age of concrete is defined as follows:

$$t_{eq} = 4000 \int_0^t \left[\frac{1}{273} - \frac{1}{T(\tau)}\right] d\tau, \tag{6}$$

where $T(\tau)$ = the temperature of concrete at τ days. The elastic modulus of concrete at t days is defined as follows:

$$E_c(t) = \beta_{cc}(t) E_{c28}. \tag{7}$$

Then, the shrinkage strains $\varepsilon_s(t, t_s)$ at an age of t days are as follows:

$$\varepsilon_s(t, t_s) = [160 + 10\beta_c(9 - 0.1 f_{cm28})] \times 10^{-6} \beta_{RH} \times \sqrt{\frac{t - t_s}{350(h/100)^2 + (t - t_s)}}, \tag{8}$$

where β_c = a shrinkage coefficient dependent on the cement type, t_s denotes the age of concrete at the beginning of shrinkage (day), and β_{RH} is related to the environmental humidity RH as follows:

$$\beta_{RH} = \begin{cases} -1.55[1 - (RH/100\%)^3] & 40\% \leq RH \leq 99\% \\ 0.5 & RH > 99\% \end{cases}. \tag{9}$$

2.2. Steel Tendon Prestress. Typically, control stress during tensioning constitutes around 25%–30% of prestress loss. Previous research has pinpointed the primary causes of prestress loss as friction between the prestressed steel bar and the pipe wall (σ_{s1}) and factors like anchor deflection, steel bar retraction, and joint compression (σ_{s2}) [8]. Given the variability in prestress tension control forces during construction, the analysis of long-term deflection and internal forces should account for variations in prestress tension and friction loss [5]. Research conducted by Zou [9] indicates that prestress loss due to excessive shrinkage of steel bars can contribute to 35.3%–52.8% of the total loss. Lin and Burns's [10] findings reveal that friction-induced prestress loss comprises over half of the total loss. Parameters within corrosion models, such as corrosion rates and rust pit sizes, are subjected to changes over time and possess inherent uncertainties, thus warranting their consideration as random variables [11]. The research of Val and Melchers [12] suggests that the radius of rust pits in a given year can be mathematically described using a specific formula as follows:

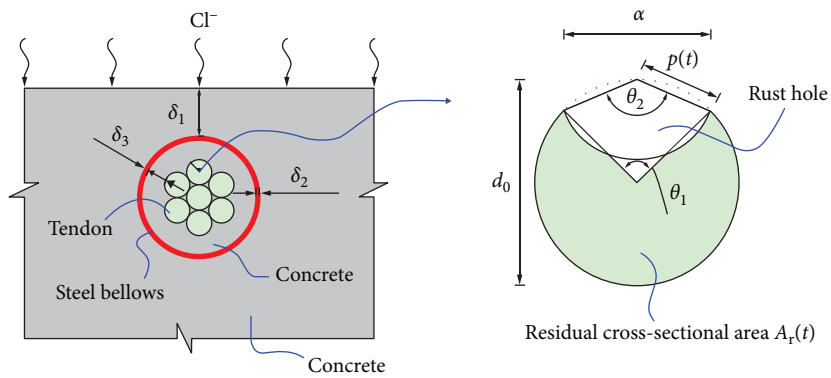

Figure 1: Diagram of steel tendon corrosion.

$$p(t)=0.0116(t-t_i)i_{corr}R, \tag{10}$$

where i_{corr} is the corrosion current density, $\mu A/cm^2$; R represents the permeability ratio, i.e., the ratio between the maximum and mean penetration.

Fick's second diffusion law can be used to calculate the initial rust time caused by chloride ion diffusion from the concrete surface to the corrugated pipe [13] as follows:

$$t_i = \frac{T_c^2}{4D}\left[\mathrm{erf}^{-1}\left(\frac{C_s - C_{cr}}{C_s}\right)\right]^{-2}, \tag{11}$$

where T_c is the concrete cover, cm; D represents the diffusion coefficient, cm^2/year; C_s denotes the chloride concentration at the concrete surface, kg/m^3; C_{cr} is the critical chloride concentration, kg/m^3; erf() represents the error function and the expression is $\mathrm{erf}(x) = \frac{2}{\sqrt{\pi}}\int_0^x e^{-t^2}dt$.

The remaining cross-sectional area after corrosion is as follows:

$$A_r(t) = \begin{cases} \dfrac{\pi d_0^2}{4} - A_1 - A_2, & p(t) \le \dfrac{\sqrt{2}}{2}d_0 \\ A_1 - A_2, & \dfrac{\sqrt{2}}{2}d_0 < p(t) \le d_0 \\ 0, & p(t) > d_0 \end{cases}. \tag{12}$$

In the formula, d_0 represents the initial diameter of the reinforcement, mm; $A_1 = \frac{1}{2}[\theta_1(\frac{d_0}{2})^2 - a|\frac{d_0}{2} - \frac{p^2(t)}{d_0}|]$, $A_2 = \frac{1}{2}[\theta_2 p^2(t) - a\frac{p^2(t)}{d_0}]$, $a = 2p(t)\sqrt{1 - [\frac{p(t)}{d_0}]^2}$, $\theta_1 = 2\arcsin(\frac{a}{d_0})$, $\theta_2 = 2\arcsin[\frac{a}{2p(t)}]$.

Darmawan and Stewart's [11] research has demonstrated that rust pits on tendons composed of seven high-strength steel wires are primarily limited to the outer surface, covering approximately half of the total surface area when considering the six external steel wires. Consequently, this article does not account for the surface corrosion of internal tendons. Compared to the regular steel bars, high-strength steel wires, along with stringent manufacturing processes, lead to a slower formation of rust pits on tendons. In cases where corrosion cracking occurs in prestressed tendons, the relative weight loss of these tendons is 1.3 times that of unstressed tendons. Hence, the section loss in Equation (12) is 1.3 times that of the unstressed tendons [14]. The determination of the initial rust time involves three components: (1) calculating the time required for chloride ion diffusion from the concrete surface to the outer surface of the corrugated metal pipe using Equation (10); (2) estimating the time necessary for the corrosion of the corrugated metal pipe with a certain thickness using Equation (11); (3) determining the distance and chloride ion diffusion time from the inner surface of the corrugated metal pipe to the outer surface of the steel bundle using Equation (10). Figure 1 illustrates the corrosion of steel tendons.

As corrosion increases, the yield strength of the steel tendon after stress degradation is [15]:

$$f_y(t) = f_{py}[1 - 100 \times \xi\eta_s(t)], \tag{13}$$

where $f_y(t)$ = the deteriorated yield strength at time t; f_{py} corresponds to its original value, which is taken as 0.88 times the ultimate strength [16]; $\eta_s(t)$ = the percentage of corrosion loss, which can be obtained from area loss. $\eta_s(t) = [A_T - A_r(t)]/A_T$, where A_T denotes the net cross-sectional area of uncorroded reinforcement, mm^2; ξ is a coefficient set to 0.0054 [15].

3. Considering the Main Girder Deflection Caused by the Web-Diagonal Cracking

When diagonal cracks appear in the web, they disrupt the structural continuity, rendering Poisson's ratio inadequate for representing the strain relationship in two orthogonal directions. Elastic theory is no longer sufficient to describe shear stiffness, necessitating the exploration of alternative methods to characterize shear stiffness degradation. To address the degradation of shear stiffness caused by diagonal cracks in webs of long-span PSC continuous box-girder bridges, Zheng et al. [17] conducted a quantitative evaluation of shear stiffness using truss theory and actual diagonal crack characteristics. The elastic shear stiffness of the structure before cracking is defined as follows:

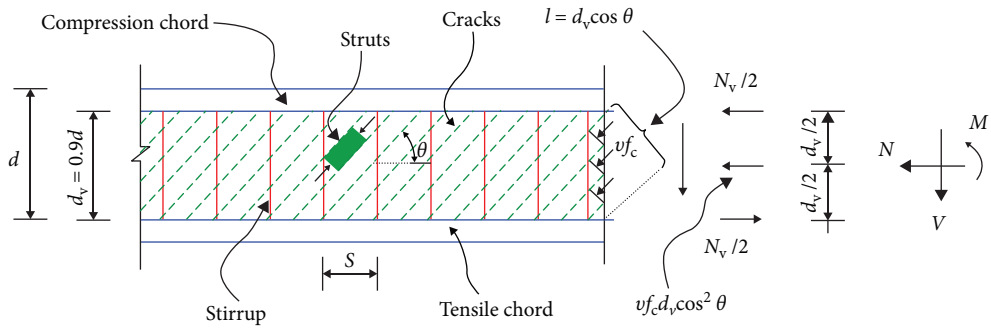

FIGURE 2: Truss model for concrete girder considering full cracking of web-diagonal cracks.

$$K_e = G_c A_v = \frac{E_c A_v}{2(1+\nu)}, \tag{14}$$

where G_c = the shear modulus of concrete, MPa; E_c represents the elastic modulus of concrete, MPa; A_v is the shear area, mm^2, taking $b_w d_v$ as a value; b_w denotes the width of the web (thickness of the web), and d_v is the effective depth of the shear zone in the truss model, which can be approximated as $0.9d$, mm; ν represents the Poisson's ratio of concrete.

When the stirrup inside the left concrete girder shears and yields, it is recommended to employ a variable angle truss model for shear analysis, taking into account the complete development of web-diagonal cracks [18]. In the model shown in Figure 2, the upper chord of the truss represents the compressed concrete zone, the lower chord represents the tensile longitudinal reinforcement, the inclined compressed strut represents the compressed concrete between diagonal cracks (green dashed line), and the vertical tensile strut represents the shear stirrups.

The shear capacity V_u is determined as the smaller value between the shear stirrup contribution V_s and the concrete contribution V_c.

$$V_s = \rho_v f_{yv} b_w d_v \cot\theta, \tag{15}$$

$$V_c = \alpha_{cw} \upsilon f_c b_w d_v \sin\theta \cos\theta, \tag{16}$$

where ρ_v = shear stirrup ratio; f_{yv} corresponds to its yield strength, MPa; θ = angle between the concrete compression strut and the beam axis perpendicular to the shear force, degree; α_{cw} is a modification factor considering the state of concrete compression in the inclined strut. υ represents effective coefficient for concrete compressive strength, which is used to account for the strength reduction of the inclined strut. It can be taken as 0.6 $(1-f_c/250)$; f_c = compressive strength of concrete, MPa.

The defined ultimate shear stiffness is as follows:

$$K_u = \frac{n\rho_v E_c A_v \cot^2\theta}{1 + n\rho_v \csc^4\theta}, \tag{17}$$

where n = the ratio of elastic modulus of the stirrup to the concrete.

The established formula for calculating the limit and elastic shear stiffness is as follows:

$$K_u = \frac{14.4\rho_v \cot^2\theta}{1 + 6\rho_v \csc^4\theta} \cdot \frac{E_c A_v}{2(1+\nu)} = \lambda_u \cdot K_e, \tag{18}$$

where λ_u represents the maximum degradation factor, equal to $14.4\rho_v \cot^2\theta/(1+6\rho_v \csc^4\theta)$.

The angle θ of the inclined strut is a crucial parameter for calculating the ultimate shear stiffness. It is determined based on the maximum strength criterion and is constrained within the range of $1 \le \cot\theta \le 2.5$. Research on shear capacity using truss models has shown that the shear strength reaches its maximum value when shear stirrup yields and the inclined concrete strut crushes (i.e., $V_s = V_c$) simultaneously. By solving Equations (15) and (16), θ can be determined as follows:

$$\cot\theta = \sqrt{\frac{\alpha_{cw} - \omega}{\omega}}, \tag{19}$$

where ω represents the strength coefficient of stirrup reinforcement, $\omega = \rho_v f_{yv}/(\upsilon f_c)$.

Eurocode 2 accounts for the effect of axial compressive stress on the angle θ using the parameter α_{cw}, which is correlated with the axial prestress stress level σ_{cp}/f_c, as illustrated in Equation (20):

$$\alpha_{cw} = \begin{cases} \dfrac{\sigma_{cp}}{f_c} + 1, & \dfrac{\sigma_{cp}}{f_c} \in [0, 0.25] \\ 1.25, & \dfrac{\sigma_{cp}}{f_c} \in [0.25, 0.5] \\ -2.5\dfrac{\sigma_{cp}}{f_c} + 2.5, & \dfrac{\sigma_{cp}}{f_c} \in [0.5, 1.0] \end{cases}. \tag{20}$$

Thus, assuming the shear stiffness after degradation under general oblique cracks to be:

$$K = \lambda \cdot K_e. \tag{21}$$

The relationship between degradation factor λ_u and cracking level G_i is as follows:

Table 1: Evaluation standard.

Level	Qualitative description	Quantitative description
1	No oblique cracks	—
2	A small amount of slight oblique cracks, with the width not exceeding the limit	The crack length is less than 1/3 of the cross-sectional dimension
3	There are many oblique cracks, and the width of the crack does not exceed the limit	The crack length is between 1/3 and 1/2 of the cross-sectional dimension
4	A large number of oblique cracks, with the width exceeding the limit	The crack length is greater than 1/2 of the cross-sectional dimension, and the mean spacing is less than 30 cm
5	A large number of oblique cracks are penetrated, and the width of the cracks is seriously exceeding the limit	Crack width greater than 1.0 mm, mean spacing less than 20 cm

$$\lambda = 1 - \frac{(1-\lambda_u)(G_i - 1)}{4}. \tag{22}$$

When the cracking level, G_1, is 1, the shear stiffness degradation factor, λ, is 1.0, and when G_1 is 5, λ equals λ_u. For other cracking levels, the shear stiffness degradation factor is determined using Equation (22). The calculation method for main girder deflection, considering diagonal web cracking, involves three steps: first, calculate the shear stiffness degradation factor; second, establish a FE analysis model; and finally, modify the Poisson's ratio of each element in the FE model to analyze the contribution of shear stiffness degradation to the main girder deflection [17]. Assuming a Poisson's ratio of 0.2 in Equation (23), the corrected Poisson's ratio can be calculated as follows:

$$\nu' = \frac{1+\nu}{\lambda} - 1 = \frac{1.2}{\lambda} - 1. \tag{23}$$

In terms of the structural composition of concrete bridge cracks, the evaluation is conducted in accordance with the 5-level criteria of the *Standards for Technical Condition Evaluation of Highway Bridges* (JTG/T H21-2011), aiming for practicality and convenience. This criterion involves a grading system consisting of five crack grades, referred to as g_{cr}, which represents the cracking severity, specifically designated as cracking grade G_i. The primary focus is on the qualitative and quantitative assessment of cracking severity through the analysis of crack width, spacing, and length [19].

Taking into account both the evaluation standard and the methodologies outlined in [17], this article integrates the features of inclined cracks to formulate a 5-level crack scale evaluation criterion for inclined cracks present in the web. When assessing the scale of diagonal cracks in accordance with Table 1, it is imperative to partition the beam segment into fundamental evaluation units, considering the bridge's segment length, which was constructed using a suspended scaffold technique. In practical applications, the determination of shear stiffness involves a systematic approach. Initially, the bridge is partitioned into distinct units. Subsequently, based on the criteria for grading oblique fractures outlined in Table 1, the respective oblique fracture scale G_i is assigned to each individual unit.

4. Case Study

The main span of the Dongming Huanghe River Highway Bridge is a PSC continuous rigid frame continuous girder composite structure system with a total length of 990 m. The span combination is $75 + 7 \times 120 + 75$m. The web thickness is 55 cm within 15 m from the root and 40 cm at midspan. The girder height varies in a parabolic fashion from 6.5 m at the pier section to 2.6 m at the midspan section. The concrete used is of grade C50, and the top and bottom prestressed tendons are made of ASTM250 grade 15.24 high-strength low-relaxation tendons with a cross-sectional area of 139 mm^2 and a standard tensile strength value of 1860 MPa. The mean distance from the concrete surface to the outer surface of the corrugated metal pipe is 10.5 cm, with a metal corrugated pipe thickness of 2.5 mm and a distance from the inner surface of the corrugated metal pipe to the outer surface of the steel bundle of 2.2 cm. The prestressed system was constructed using the posttensioning method with a tensioning control stress of 1395 MPa and a concrete age of 28 days during tensioning. In 2003, an external prestressing tendon was added to the bottom plate to improve the stress at the lower edge of the bottom plate. This was done using 15.24 nonadhesive galvanized tendons with a tensile control stress of 1276 kN. To address insufficient shear bearing capacity and midspan deflection, the main girder was reinforced with a SCS in 2014. Eight jacks were used for tensioning the stay cables from the middle tower (61# and 62#) to the side tower (58# and 65#), and the stay cables were symmetrically tensioned in batches in a sequence from long to short. The design cable force values for the long and short cables were 2.7 and 2.1 MN, respectively. The tensioning process was divided into six levels based on 30%, 50%, 65%, 75%, 85%, and 90% of the tensioning control force [20]. Figures 3 and 4 illustrate the layout dimensions of the main girder and the cross-sectional dimensions of the box girders at the root and midspan.

4.1. Selection of Random Variables. This paper does not consider the randomness of theoretical thickness due to the small difference between actual size and theoretical thickness of the box-girder section. The temperature at which deflection data are collected is relatively constant, ranging from 21 to 25.5°C, and its impact on deflection can be ruled out. During model validation, parameters related to phase II dead load and the residual value of external tendon prestress

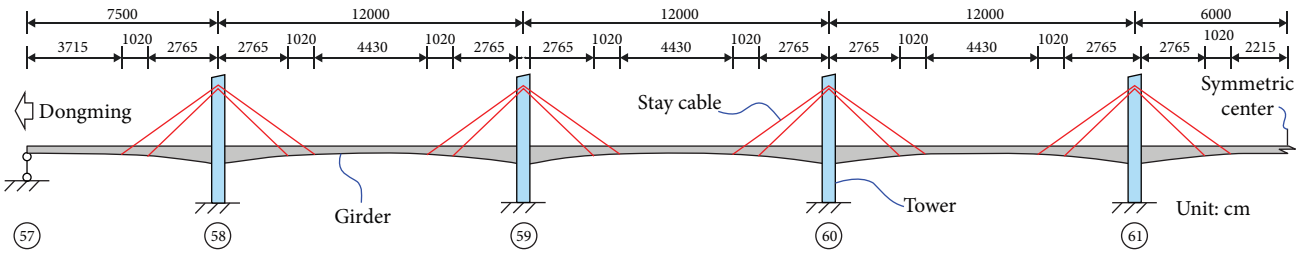

Figure 3: Dimensions of main girder of Dongming Huanghe River Highway Bridge.

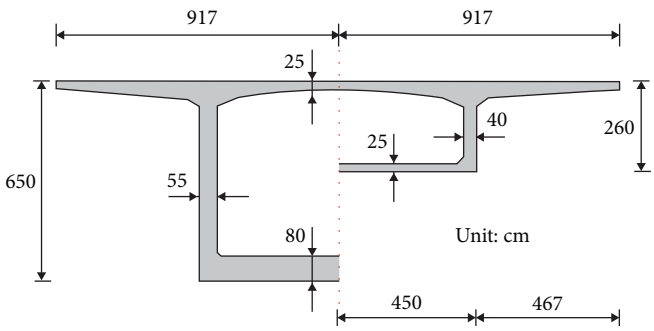

Figure 4: Root and midspan cross-sectional dimensions.

are based on design or measured results [21, 22], and random variables are not considered. The model does not consider deflection caused by normal cracks since, according to the crack detection results in 2002, 75.99% of the total 3066 cracks found in the main girder were oblique cracks mainly distributed on the web [23]. The deflection caused by web-diagonal cracking is treated as a deterministic factor, and the impact of carbon fiber reinforcement of top and bottom plates in 2003 is not considered. The dead weight of the thickened web section and the ordinary reinforcement is simplified as the dead load of the main bridge. Table 2 lists the 19 selected random variables.

4.2. Evaluation of Oblique Cracks and Calculation of Shear Stiffness Degradation Factor. The parameters used to calculate the shear stiffness degradation factor in this paper: $f_c = 50$ MPa, $f_{yv} = 335$ MPa, and the shear stirrup ratio ρ_v of the pier and midspan box girder are 1.02% and 1.21%, respectively. The mean compressive stress σ_{cp} of the concrete at the root and midspan of the box girder is 11.72 and 8.51 MPa, respectively. If $\overline{\sigma}_{cp} = 10.12 < 12.5$ MPa, a correction factor $\alpha_{cw} = 1 + 10.12/5 = 1.02$ is selected. The effective coefficient of concrete compressive strength $\upsilon = 0.6(1 - f_c/250)$, then $\upsilon = 0.48$. According to $\omega = \rho_v f_{yv}/\upsilon f_c$, the calculated strength coefficient of stirrup $\omega = 0.17$. According to $\cot\theta = \sqrt{(\alpha_{cw} - \omega)}/\omega = 2.46$, $\theta = 22.12°$, and $\lambda_u = 0.228$. Substitute the above parameters into Equations (18) and (19) to calculate the shear stiffness degradation factor and the modified Poisson's ratio at all levels of oblique crack scale. The specific calculation results are shown in Table 3. The evaluation results of web-oblique crack in 2002 and 2008 are listed in Tables 4 and 5, respectively.

4.3. Deflection Caused by the Web-Diagonal Cracking. The MIDAS/Civil general FE analysis software was used in this study. Since the deflection of the bridge is mainly longitudinal and vertical, the FE model uses beam elements for the main girder (347 in total), beam element models for the piers (312 in total), and truss elements for the stay cables (64 in total). The displacement boundary conditions of the model are all rigid constraints without considering elastic boundary conditions. The main girder and the stay cable are elastically connected. Figure 5 illustrates the FE computational model.

Two models were used in this study: Model A, which did not account for the deflection of the main girder caused by web-diagonal cracks, and Model B, which did. Figure 6 shows a comparison of the main girder deflection calculated using both models in 2002 and 2008. L represents the distance from the center of the 57# pier. The relative error is defined as $[(W - W')/W] \times 100\%$, the average absolute error is defined as $[\sum_{i=1}^{N} |(W - W')/W|/N] \times 100\%$, W denotes the measured value, W' represents the calculated value, and N is number of measuring points.

Compared to Model A, Model B yielded calculated results that were closer to the measured values, with smaller errors. The mean absolute error of Model A in 2002 was 23.56%, while that of Model B was 17.51%. In 2008, the mean absolute error of Model A was 44.67%, while that of Model B was 33.67%. Considering the contribution of diagonal web cracking to the deflection of the main girder, the mean deflection of the main girder over 2 years accounted for 8.8% of the total deflection. The study indicates that the calculated value using truss theory is closer to the measured value, and the degree of diagonal cracking of the web has a significant impact on shear deflection. Therefore, the deflection caused by web-diagonal cracking cannot be ignored.

4.4. Uncertainty and Sensitivity Analysis of Long-Term Deflection. To improve sampling efficiency, Iman and Conover proposed the Latin hypercube sampling (LHS) method, a multidimensional and uniform sampling technique that enhances the computational efficiency of the MCS method [33]. This method avoids repeated sampling and ensures that the sampling values cover the entire distribution range of input variables, reflecting the overall variation rule with a small sample size. In this study, the LHS random simulation method is used to sample 19 random variables, with a sample size of 57, and input them into the model for long-term deflection increment analysis. The state after the completion of bridge deck pavement in 1993 is taken as the initial reference state. Due to space constraints, the deflection values of the 59# and 60# spans in the model are selected for

Table 2: Statistical properties of random variables.

Variable	Properties	Distribution	Mean	COV	Source
DLA	Dynamic load amplification/X1	Normal	1.0899	0.0279	GBT 50283-1999 [24]
K_{SQ}	Ratio of maximum measured value to design value/X2	Extremum I type	0.7995	0.0862	
α_1	Creep uncertainty coefficient/X3	Normal	1.000	0.34	Pan et al. [25]
α_2	Shrinkage uncertainty coefficient/X4	Normal	1.000	0.45	
f_{cm28} (MPa)	Compressive strength (28 days)/X5	Normal	49.2	0.066	Yang [1]
E_{c28} (MPa)	Elastic modulus of concrete (28 days)/X6	Normal	34,500	0.04	Guo et al. [26]
DW_1 (kN/m^3)	Density of concrete/X7	Normal	26.5	0.215	
T (°C)	Annual mean temperature/X8	Normal	23.9	0.341	CMDC [27]
RH (%)	Annual relative humidity/X9	Normal	70.9	0.175	
f_{py} (MPa)	Yield strength/X10	Normal	1636.8	0.025	AL-Harthy et al. [28]
σ_{con} (MPa)	Prestressed tension control stress/X11	Normal	1,395	0.040	
σ_{s2} (MPa)	Anchorage deflection, reinforcement retraction, and joint compression/X12	Normal	5.549	0.175	Fan et al. [29]
μ	Friction coefficient/X13	Normal	0.18	0.299	Pan [5]
k	Friction influence coefficient/X14	Normal	0.003	0.553	
C_s (kg/m^3)	Surface chloride concentration/X15	Normal	15	0.2	Val et al. [30]
C_{cr} (kg/m^3)	Critical chloride concentration/X16	Normal	2.0	0.2	
D (cm^2/year)	Diffusion coefficient/X17	Lognormal	0.631	0.2	
i_{corr} (μA/cm^2)	Corrosion current density/X18	Normal	1.0	0.2	González et al. [31]
R	Permeability ratio/X19	Normal	3.0	0.33	Stewart et al. [32]

Table 3: Parameter values of different cracked grades.

G_i	λ	ν'
1	1.000	0.200
2	0.807	0.487
3	0.614	0.954
4	0.421	1.850
5	0.228	4.260

Table 4: Evaluating grade of web oblique crack in 2002.

No.	Segmental oblique crack scale (g_{cr})																								
	1	2	3	4	5	6	7	8	9	10	11	12	13	13′	12′	11′	10′	9′	8′	7′	6′	5′	4′	3′	2′	1′
59#	1	1	1	2	2	3	3	3	2	1	1	1	1	1	1	2	3	2	3	2	3	1	1	1	1	1
60#	1	1	1	1	4	2	2	3	2	2	2	1	1	1	1	2	2	1	2	3	3	2	1	1	1	1
61#	1	1	1	1	4	3	2	3	1	1	2	1	1	1	1	2	2	3	1	1	3	2	1	1	1	1
62#	1	1	1	1	1	4	3	3	2	2	1	1	1	1	1	2	2	1	1	2	2	1	1	1	2	1
63#	1	1	1	1	1	1	1	1	2	2	2	1	1	1	1	1	2	2	2	2	1	1	1	1	1	1
64#	1	1	1	1	2	1	2	3	3	2	2	1	1	1	1	1	2	2	2	3	1	1	1	1	1	1
65#	1	1	1	1	1	2	3	2	3	3	2	1	1	1	2	3	1	1	1	2	3	2	1	1	1	1
	—	—	—	—	—	—	—	—	18′	17′	16′	15′	14′	13′	12′	11′	10′	9′	8′	7′	6′	5′	4′	3′	2′	1′
58#	—	—	—	—	—	—	—	—	1	1	1	1	1	1	1	1	1	1	1	1	1	1	1	1	1	1
66#	—	—	—	—	—	—	—	—	1	1	1	1	1	1	1	1	1	2	2	2	1	2	1	1	1	1

comparison. Figure 7 shows the calculated midspan deflection values of the 59# and 60# spans for 57 models.

In the figure, the mean value curves (blue curves) for spans 59# and 60# represent the deflection values calculated when using the mean values of variables (from the fourth column in Table 2) as input values for the FE model. These curves depict the deflection profiles obtained through calculations with these mean input values. From the figure, it can

Table 5: Evaluating grade of web oblique crack in 2008.

No.	Segmental oblique crack scale (g_{cr})																								
	1	2	3	4	5	6	7	8	9	10	11	12	13	13′	12′	11′	10′	9′	8′	7′	6′	5′	4′	3′	2′	1′
59#	1	3	1	1	1	4	4	3	2	1	1	1	1	1	2	2	2	3	3	2	3	3	1	2	1	1
60#	1	1	1	1	4	2	2	3	2	2	1	1	1	1	1	1	2	1	3	4	3	2	1	1	1	1
61#	1	1	1	1	4	2	2	3	2	1	1	1	1	1	1	1	2	3	2	3	3	2	2	1	1	1
62#	1	1	1	1	3	2	3	3	2	2	1	1	1	1	1	1	2	1	2	2	2	2	1	1	3	2
63#	1	1	1	1	2	2	2	2	2	1	1	1	1	1	1	1	1	1	2	2	1	2	2	1	1	2
64#	2	1	1	2	2	2	2	3	2	2	2	1	1	1	1	1	2	2	2	2	1	1	1	1	2	2
65#	1	1	1	1	1	1	3	1	2	2	1	1	1	1	2	1	1	2	1	2	2	2	1	1	1	1
	—	—	—	—	—	—	—	—	18′	17′	16′	15′	14′	13′	12′	11′	10′	9′	8′	7′	6′	5′	4′	3′	2′	1′
58#	—	—	—	—	—	—	—	—	1	1	2	1	1	1	3	1	1	1	1	1	1	1	1	1	1	1
66#	—	—	—	—	—	—	—	—	2	2	1	1	1	1	2	1	1	2	2	2	1	2	1	1	1	1

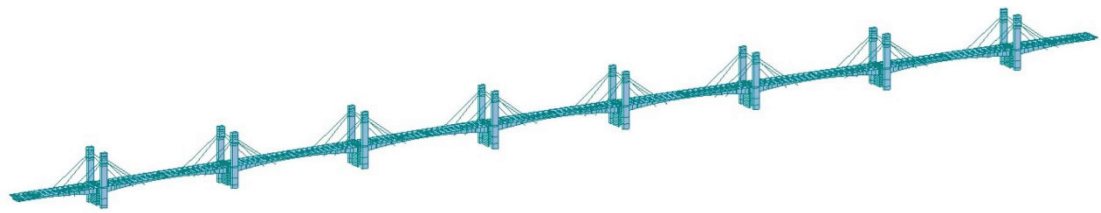

Figure 5: FE computational model.

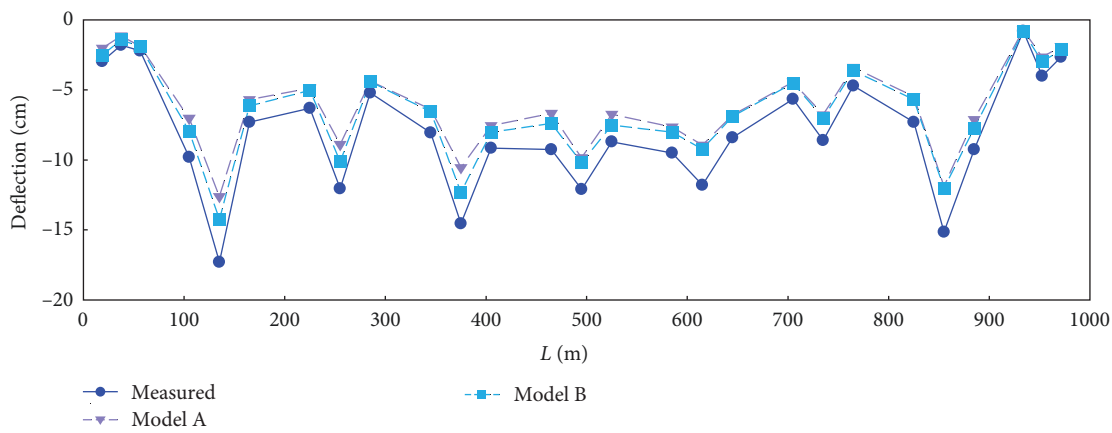

(a)

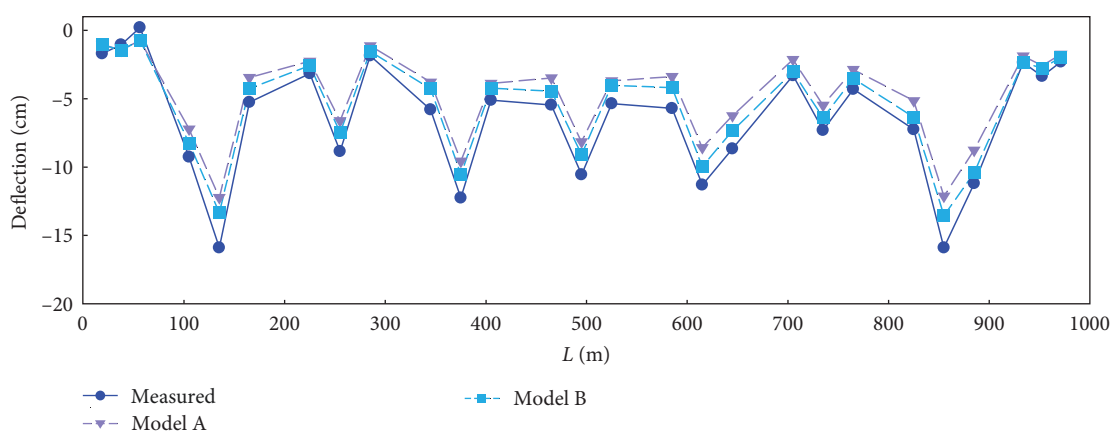

(b)

Figure 6: Contrast diagrams of main girder deflection in (a) 2002 and (b) 2008.

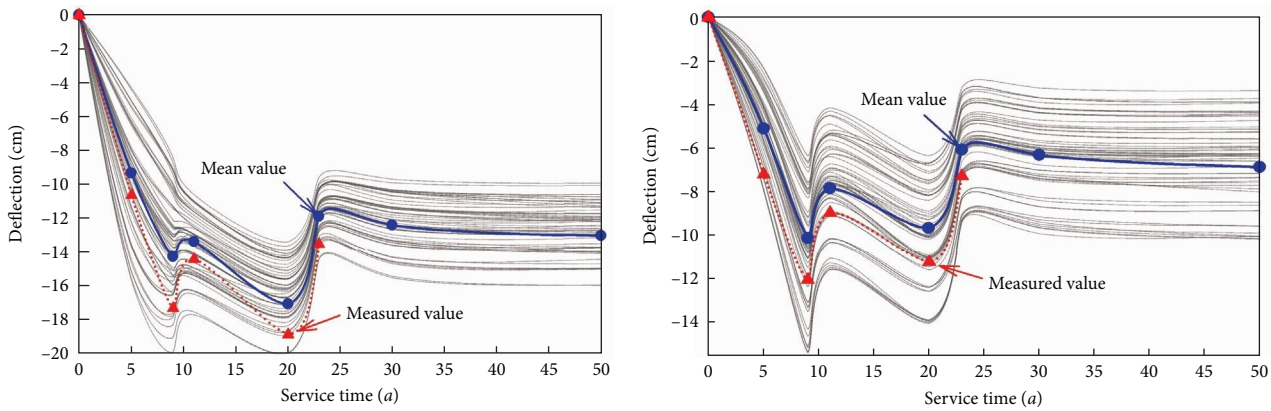

Figure 7: Calculated values of midspan deflection of (a) 59# and (b) 60#.

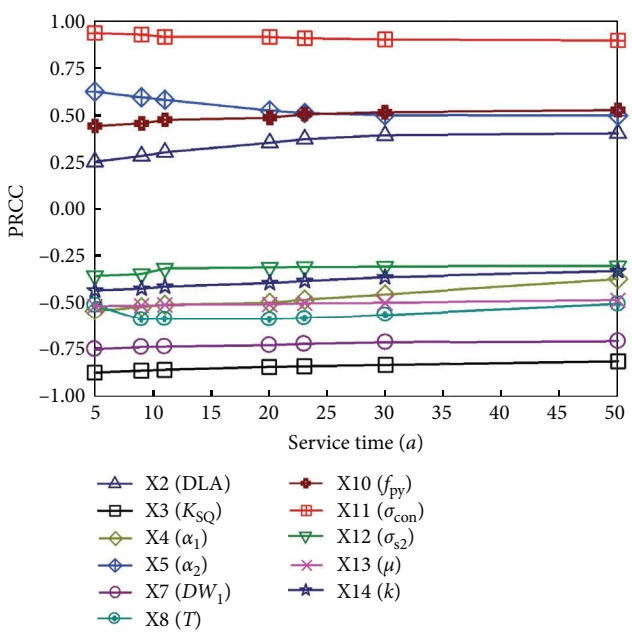

Figure 8: Sensitivity of calculation parameters.

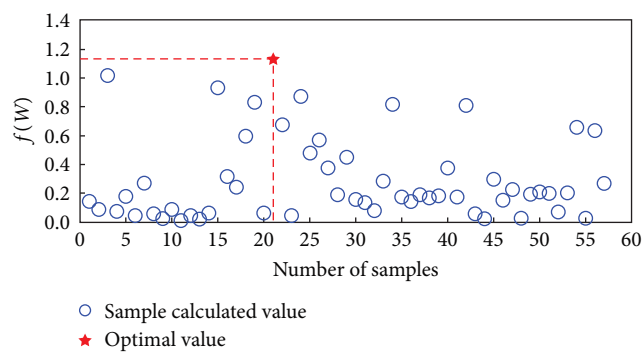

Figure 9: Calculated values of object function of 57 samples.

be observed that the calculated results obtained from the mean model significantly differ from the measured values. Therefore, it is challenging to reveal the variation pattern of the main girder deflection using a FE model established by deterministic parameters. Due to differences in the effects of concrete shrinkage, creep, concrete modulus of elasticity, and prestress, the long-term deflection is complex, making it difficult to reveal the changing rules of main girder deflection using FE models established with deterministic parameters. However, the deflection law of the midspan is consistently observed, and the reinforcement effect is relatively obvious. In 2016, the maximum lifting amount of the main girder after applying SCS was 5.61 cm. After 27 years of SCS reinforcement (i.e., 50 years of bridge operation), the maximum deflection values of the 59# and 60# spans were 15.89 and 10.14 cm, respectively. The long-term deflection is mainly completed at an early stage, so for PSC continuous box-girder bridges constructed in segments, the early concrete curing time should be sufficient. During the uncertainty analysis of random variables for the long-term deflection, the input values of the 19 random variables were varied. In order to consider the interaction between the input random variables and avoid errors caused by deterministic sensitivity analysis, the partial rank correlation coefficient (PRCC) of different influencing factors of long-term deflection was further analyzed [34]. The specific calculation results are shown in Figure 8.

Figure 8 shows that, for a 5-year operation period, the PRCC ranking of the five most important parameters that affect the long-term deflection are: prestressed tension control stress (0.936), creep uncertainty coefficient (−0.868), density of concrete (−0.745), compressive strength (28 days) (0.626), and shrinkage uncertainty coefficient (−0.536). From the perspective of PRCC for different operating years, the PRCC for prestressed tension control stress, creep uncertainty coefficient, and density of concrete are relatively large. The PRCC of the prestressed tension control stress is positive, indicating that as the prestressed tension control stress increases, the response becomes greater, but the deflection development is negative, meaning that the development of deflection becomes smaller. The PRCC of the creep uncertainty coefficient and the density of concrete is negative, indicating that as the creep uncertainty coefficient and the density of concrete increase, the response becomes smaller, and the development of deflection becomes

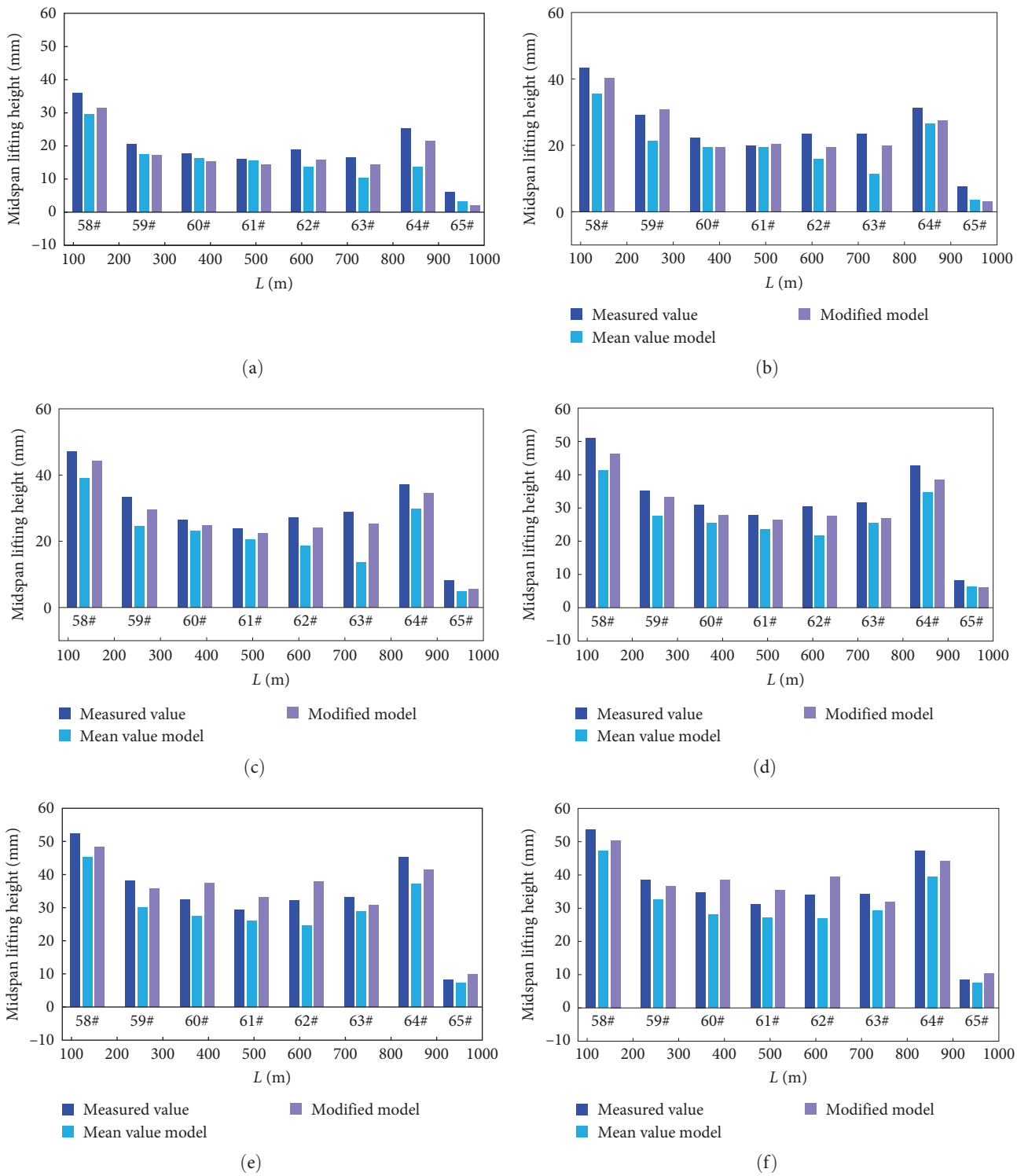

Figure 10: Comparisons between calculated and measured values of midspan uplift under different models. (a) 0.3P, (b) 0.5P, (c) 0.65P, (d) 0.75P, (e) 0.85P, and (f) 0.9P.

greater. Therefore, it is crucial to strictly control the longitudinal tension and stress control of prestressed tendons during the construction phase. High-strength and lightweight concrete can also be used in the design to control excessive deflection of the girder. Additionally, creep is one of the uncertain properties of concrete, and the random influence of creep coefficient cannot be ignored when analyzing the long-term deflection.

The determination of the initial corrosion time of the tendon, calculated using the mean value, involves the

following considerations: (1) the diffusion time for chloride ions to travel a distance of 10.5 cm from the concrete surface to the outer surface of the corrugated metal pipe is denoted as t_1 and equals 38.77 years; (2) the time required for the corrosion of the 2.5-mm thick corrugated metal pipe is represented by t_2, which amounts to 7.18 years; (3) the diffusion time for corrosion to propagate from the inner surface of the corrugated metal pipe, situated 2.2 cm from the outer surface of the steel beam, to the beam's outer surface is denoted as t_3 and amounts to 1.70 years. Consequently, the calculated estimate for the initial rusting period, based on the mean model, is approximately 48 years. Subsequently, employing Equation (12), the remaining sectional area following corrosion is computed, resulting in a corrosion loss percentage of 0.28%. Correspondingly, the yield strength of the tendon after undergoing stress degradation is determined to be 1634.3 MPa. Importantly, this reduction in yield strength due to tendon stress degradation proves to be marginal when juxtaposed with the original yield strength of 1636.8 MPa. Notably, upon careful analysis, it is established that the deformation encountered by the girder as a consequence of tendon corrosion remains inconsequential throughout a 50-year operational span.

4.5. Selection of Optimal Combination Parameters and Result Comparison. The objective function plays a crucial role in evaluating the degree to which individuals in a population reach or approach the optimal solution, and is used as a basis for natural selection of the population. Therefore, the construction of objective functions is crucial for obtaining optimal solutions or genetic individuals with high accuracy. In this study, the objective function is assumed to be the sum of the square of the relative difference between the target test value and the FE calculation value, which can be expressed as follows:

$$F(W) = \sum_{j=1}^{m}\sum_{i=1}^{n}\left(\frac{W_{i,j} - W'_{i,j}}{W_{i,j}}\right)^2. \tag{24}$$

Then, the defined objective function value is as follows:

$$f(W) = \frac{1}{\sqrt{F(W)/20}}, \tag{25}$$

where $W_{i,j}$ represents the measured deflection value at the i measuring point in the j-th operating year; $W'_{i,j}$ is the calculated value of deflection at the i measuring point for the j-th operating year; m denotes the number of operating years actually investigated, with this article specifically selecting the 9th, 11th, and 20th operating years, resulting in $m = 3$; n is the number of selected measurement points. We utilized the midspan measurement points, which range from 58# to 65#, totaling seven points; thus, $n = 7$.

Based on the calculation results of the 57 samples, the maximum value of the objective function is, and the corresponding optimal sample parameters are 1.13, 0.79, 0.57, 1.21, 51.25, 35910.78, 26.87, 22.07, 6.46, 1591.06, 1310.71, 6.38, 0.16, 0.0012, 12.20, 2.47, 1.72, 1.05, and 4.73. Figure 9 shows the calculated values of the objective function for 57 samples.

The optimal sample parameter FE model (modified FE model) is used to conduct a deterministic analysis of the structural performance of the main girder during the SCS tensioning phase. Figure 10 compares calculated and measured midspan uplift values under different models. The mean absolute error of midspan deflection calculated by the modified model is 13.70%, while that of the mean model is 21.69%. In summary, the modified model yields prediction results for the deflection of the main girder that are closer to the measured values, and its prediction accuracy is better than the mean model.

5. Conclusions

This paper presents a deflection prediction model of PSC box-girder enhanced by SCS during the tensioning phase. Based on this study, the following conclusions can be drawn:

(1) Considering the web-diagonal cracking, the calculated mean shear deflection, which accounts for 8.8% of the total deflection, is closer to the measured value. Therefore, the deflection caused by web-diagonal cracking cannot be ignored.

(2) Due to differences in the effects of concrete shrinkage, creep, elastic modulus of concrete, and prestress, the calculated results of the generated stochastic FE model differ greatly. The long-term deflection of PSC box-girder bridges is mainly completed at an early stage, therefore, for bridges constructed in segments, sufficient early concrete curing time should be ensured.

(3) The partial correlation coefficients of the prestressed tension control stress, creep uncertainty coefficient, and density of concrete are relatively large. Among them, the prestressed tension control stress is positively correlated with the service life, indicating that an increase in the prestressed tension control stress is associated with a reduction in the development of deflection. The creep uncertainty coefficient and density of concrete are negatively correlated with the service life, indicating that as the creep uncertainty coefficient and density of concrete continue to increase, the development of the deflection becomes greater.

(4) The modified model yields prediction results for the main girder deflection that are closer to the measured values, and its prediction accuracy is significantly better than the mean model. The modified model can better evaluate the mechanical properties of the main beam before and during the tensioning stage of cable-stayed reinforcement, based on the selection of optimal parameters and detailed testing data.

Data Availability

All data generated or analyzed during this study are included within the article.

Conflicts of Interest

The authors declare that they have no conflicts of interest.

Authors' Contributions

Gangnian Xu conceptualized the study, developed the methodology, supervised the study, carried out funding acquisition, wrote the original draft, and reviewed and edited the manuscript. Weimin Xu developed the methodology, administrated the project, and reviewed and edited the manuscript. Zhanhong Wang developed the methodology and edited the manuscript. Ruishuo Zhang analyzed using software, carried out formal analysis, wrote the original draft, and visualized the study.

Acknowledgments

This work is supported by the Shandong Provincial Department of Transportation Science and Technology Plan Project (Nos. 2020B92 and 2023B94) and the Open Project of Key Laboratory of Transportation Industry (Beijing) for Old Bridge Detection and Reinforcement Technology (No. 2021-JQKFKT-3).

References

[1] I. H. Yang, "Uncertainty and sensitivity analysis of time-dependent effects in concrete structures," *Engineering Structures*, vol. 29, no. 7, pp. 1366–1374, 2007.

[2] T. Guo and Z. Chen, "Deflection control of long-span PSC box-girder bridge based on field monitoring and probabilistic FEA," *Journal of Performance of Constructed Facilities*, vol. 30, no. 6, 2016.

[3] T. Guo, T. Liu, and A. Li, "Deflection reliability analysis of PSC box-girder bridge under high-speed railway loads," *Advances in Structural Engineering*, vol. 15, no. 11, pp. 2001–2011, 2012.

[4] T. Guo, R. Sause, D. M. Frangopol, and A. Li, "Time-dependent reliability of PSC box-girder bridge considering creep, shrinkage, and corrosion," *Journal of Bridge Engineering*, vol. 16, no. 1, pp. 29–43, 2011.

[5] Z.-F. Pan, "Time dependent deflection of long-span prestressed concrete box girder bridge," Nanjing, China, 2013.

[6] CEB-FIP, *CEB-FIP Model Code 1990: Design Code*, Thomas Telford, London, 1994.

[7] Z.-P. Bažant, Q. Yu, G. Li, G.-J. Klein, and V. Krístek, "Excessive deflections of record-span prestressed box girder: lessons learned from the collapse of the Koror–Babeldaob Bridge in Palu," *ACI Concrete International*, vol. 32, pp. 44–52, 2010.

[8] Y.-P. Song, Y. Che, D.-Y. Ma, and G.-P. Zhao, "Study on losses of prestress due to friction for curved prestressing tendon," *China Civil Engineering Journal*, vol. 35, pp. 105–108, 2002.

[9] H.-Q. Zou, *Study on Crack Control of Long-Span Prestressed Concrete Continuousrigid Frame Bridge during Construction Period*, Hunan University, Changsha, 2016.

[10] T.-Y. Lin and N.-H. Burns, "Design of prestressed concrete structures," 1983.

[11] M.-S. Darmawan and M.-G. Stewart, "Spatial time-dependent reliability analysis of corroding pretensioned prestressed concrete bridge girders," *Structural Safety*, vol. 29, pp. 16–31, 2007.

[12] D. V. Val and R. E. Melchers, "Relibality of deteriorating RC slab bridges," *Journal of Structural Engineering*, vol. 123, no. 12, pp. 1638–1644, 1997.

[13] M. Enright and D. Frangopol, "Probabilistic analysis of resistance degradation of reinforced concrete bridge beams under corrosion," *Engineering Structures*, vol. 20, pp. 960–971, 1998.

[14] F. Li, Y. Yuan, and C.-Q. Li, "Corrosion propagation of prestressing steel strands in concrete subject to chloride attack," *Construction and Building Materials*, vol. 25, no. 10, pp. 3878–3885, 2011.

[15] Y. G. Du, L. A. Clark, and A. H. C. Chan, "Residual capacity of corroded reinforcing bars," *Magazine of Concrete Research*, vol. 57, no. 3, pp. 135–147, 2005.

[16] S.-A. Mirza, D.-K. Kikuchi, and J.-G. Macgregor, "Flexural strength reduction factor of bonded prestressed concrete beams," *American Concrete Institute*, vol. 77, no. 4, pp. 237–246, 1980.

[17] K.-Q. Zheng, Z. Liu, Y.-F. Zhang, and S.-Q. Qin, "Shear stiffness assessment method for concrete girder bridges with web diagonal cracks," *Bridge Construction*, vol. 45, pp. 46–50, 2015.

[18] BS EN, *Eurocode 2: Design of Concrete Structures-Part 1-1. General Rules and Rules for Buildings*, European Committee for Standardization, Brussels, Belgium, 2004.

[19] J.T.G./T.H21-2011, *Standards for Technical Condition Evaluation of Highway Bridges*, China Communications Press, Beijing, China, 2011.

[20] G.-N. Xu, Y.-Z. Wang, S.-M. Wang, and L.-Y. Wang, "Key construction techniques for strengthening of main girder of Dongming Huanghe River Highway Bridge," *Bridge Construction*, vol. 47, no. 5, pp. 101–106, 2017.

[21] M. Qapo, S. Dirar, J. Yang, and M. Z. E. B. Elshafie, "Nonlinear finite element modelling and parametric study of CFRP shear-strengthened prestressed concrete girders," *Construction and Building Materials*, vol. 76, pp. 245–255, 2015.

[22] A. Bezuglov and G. Comert, "Short-term freeway traffic parameter prediction: application of grey system theory models," *Expert Systems with Applications*, vol. 62, pp. 284–292, 2016.

[23] J.-J. Wei, "Shrinkage and creep effect of three-span continuous variable cross-section prestressed concrete bridge," *Journal of Xi'an University of Science and Technology*, vol. 35, pp. 192–196, 2015.

[24] GBT 50283-1999, *Unified Standard for Reliability Design of Highway Engineering Structures*, China Planning Press, Beijing, China, 1999.

[25] Z.-F. Pan, Z.-T. Lv, Z. Liu, and S.-P. Meng, "Uncertainty analysis of creep and shrinkage effect in continuous rigid frame of Sutong Bridge," *Journal of Engineering Mechanics*, vol. 26, pp. 67–73, 2009.

[26] T. Guo, Z. Chen, T. Liu, and D. Han, "Time-dependent reliability of strengthened PSC box-girder bridge using phased and incremental static analyses," *Engineering Structures*, vol. 117, pp. 358–371, 2016.

[27] CMDC, "China Meteorological Data Service Centre," 2008, http://data.cma.cn/.

[28] A.-S. AL-Harthy and D.-M. Frangopol, "Reliability-based design of prestressed concrete beams," *Engineering Structures*, vol. 120, pp. 3156–3177, 1994.

[29] J. Fan, F. Zhang, L. Gao, D. Wang, and H. Gao, "Rebar retraction probability distribution model of prestressed clip anchor," *Journal of Chongqing Jiaotong University (Natural Science)*, vol. 38, pp. 9–13, 2019.

[30] D. V. Val and P. A. Trapper, "Probabilistic evaluation of initiation time of chloride-induced corrosion," *Reliability Engineering & System Safety*, vol. 93, no. 3, pp. 364–372, 2008.

[31] J. A. González, C. Andrade, C. Alonso, and S. Feliu, "Comparison of rates of general corrosion and maximum pitting penetration on concrete embedded steel reinforcement," *Cement and Concrete Research*, vol. 25, no. 2, pp. 257–264, 1995.

[32] M.-G. Stewart and D.-V. Rosowsky, "Time-dependent reliability of deteriorating reiforced concrete bridge decks," *Structure Safety*, vol. 20, pp. 91–109, 1998.

[33] R. C. Iman and W. J. Conover, "Small sample sensitivity analysis techniques for computer models with an application to risk assessment," *Communications in Statistics—Theory and Methods*, vol. 9, no. 17, pp. 1749–1842, 1980.

[34] Y.-T. Zhang and S.-P. Meng, "Prediction of long-term deflection of long-span continuous rigid-frame bridges using the response surface method," *China Civil Engineering Journal*, vol. 44, pp. 102–106, 2011.